Journal of Applied Physics

RESEARCH ARTICLE | APRIL 03 2024

Estimating the lattice thermal conductivity of AlCoCrNiFe high-entropy alloy using machine learning

Special Collection: Machine Learning for Thermal Transport

Jie Lu ; Xiaona Huang ; Yanan Yue

J. Appl. Phys. 135, 135104 (2024)
https://doi.org/10.1063/5.0201042

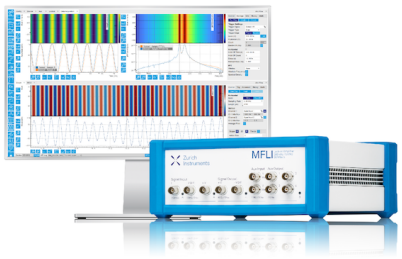

Journal of Applied Physics ARTICLE pubs.aip.org/aip/jap

Estimating the lattice thermal conductivity of AlCoCrNiFe high-entropy alloy using machine learning

Cite as: J. Appl. Phys. **135**, 135104 (2024); doi: 10.1063/5.0201042
Submitted: 29 January 2024 · Accepted: 19 March 2024 ·
Published Online: 3 April 2024

Jie Lu, Xiaona Huang,[a] and Yanan Yue[a]

AFFILIATIONS

School of Power and Mechanical Engineering, Wuhan University, Wuhan, Hubei 430072, China

Note: This paper is part of the special topic, Machine Learning for Thermal Transport.
[b]**Authors to whom correspondence should be addressed:** xnhuang@whu.edu.cn and yyue@whu.edu.cn

ABSTRACT

The lattice thermal conductivity stands as a pivotal thermos-physical parameter of high-entropy alloys; nonetheless, achieving precise predictions of the lattice thermal conductivity for high-entropy alloys poses a formidable challenge due to their complex composition and structure. In this study, machine learning models were built to predict the lattice thermal conductivity of AlCoCrNiFe high-entropy alloy based on molecular dynamic simulations. Our model shows high accuracy with R^2, mean absolute percentage error, and root mean square error of the test set is 0.91, 0.031, and 1.128 W m^{-1} k^{-1}, respectively. In addition, a high-entropy alloy with low a lattice thermal conductivity of 2.06 W m^{-1} k^{-1} ($Al_8Cr_{30}Co_{19}Ni_{20}Fe_{23}$) and with a high lattice thermal conductivity of 5.29 W m^{-1} k^{-1} ($Al_{0.5}Cr_{28.5}Co_{25}Ni_{25.5}Fe_{20.5}$) was successfully predicted, which shows good agreement with the results from molecular dynamics simulations. The mechanisms of the thermal conductivity divergence are further explained through their phonon density of states and elastic modulus. The established model provides a powerful tool for developing high-entropy alloys with the desired properties.

I. INTRODUCTION

In contrast to conventional metal alloys, which typically depend on just one major element, high-entropy alloys (HEAs) consist of a homogeneous blend of at least five or more elements.[1] Its distinctive crystal structure and chemical composition confer upon it numerous excellent properties,[2,3] including exceptional mechanical characteristics[4] and high-temperature stability.[5] Lattice thermal conductivity is a significant thermo-physical parameter of HEAs materials, directly impacting the thermal conduction efficiency and thermal management performance of the materials.[6] Accurately predicting the lattice thermal conductivity of HEAs is challenging due to the presence of a variety of major elements in HEAs and the significantly higher number of possible compositions compared to conventional alloys.[7] Although capable of measuring the thermal conductivity of HEAs, conventional experimental methods are laborious, time-consuming, and expensive.[8,9] Moreover, equilibrium and non-equilibrium molecular dynamics (NEMD) simulations are constrained by the requirement for empirical potentials to depict the interactions between atoms.[10,11] Similarly, first-principles combined with phonon Boltzmann transport equation calculations demand substantial computational resources.[12] Therefore, it is necessary to find an effective and rapid method to predict the lattice thermal conductivity of HEAs.[13] Machine learning (ML) can extract underlying regularities from the intricate structures of HEAs, comprised of multiple elements, facilitating rapid and precise prediction of thermal conductivity.[14,15] Wu *et al.*[16] employed ML models to predict the thermal conductivity of polymers and achieved the successful synthesis of novel polymers exhibiting high thermal conductivity,[17,18] while also offering novel concepts and methodologies for enhancing material properties.[19–21]

However, achieving the ML prediction of thermal conductivity for HEAs is not always straightforward.[22–24] The intricacies of the highly complex chemical composition and crystal structure of HEAs result in a high data dimensionality and a dearth of data samples,

posing challenges for the training and generalization of ML models.[25–27] Sun *et al.*[28] calculated the lattice thermal conductivity of Al0.3CoCrFeNi by the NEMD method, and the calculated values were similar to the experimentally measured values. It is demonstrated that the NEMD method can accurately calculate the lattice thermal conductivity of HEAs. The advantage of integrating molecular dynamics (MD) with ML for predicting the lattice thermal conductivity of HEAs resides in the NEMD method's capacity to furnish a substantial amount of precise lattice thermal conductivity data, which the ML model can leverage for training and prediction, thereby achieving an efficient and accurate prediction of the lattice thermal conductivity of HEAs.[29,30] This synergistic approach can mitigate the limitations of the NEMD method, which is confined to a restricted number of components, and expand its prediction capacity to a range of alloys containing more components.[31,32] Moreover, the ML model can offer a more profound comprehension of the intricate correlations of the thermal conductivity of HEAs, thereby presenting additional opportunities for material design and optimization.[33]

In this study, we present an ML method capable of predicting the lattice thermal conductivity of AlCoCrNiFe at the MD level of accuracy. Calculation of the Pearson coefficient between the input and output values of the ML model revealed that the variation in aluminum content has the most significant effect on the lattice thermal conductivity. The variation of the lattice thermal conductivity was further analyzed by calculating its phonon state density and elastic modulus. Our method will expedite the determination of lattice thermal conductivities of AlCoCrNiFe of varying compositions, thereby advancing the development of HEAs with excellent properties.

II. METHODS

A. Modeling of HEAs

We directly modeled and ran the subsequent calculation in the Large-scale Atomic/Molecular Massively Parallel Simulator Package.[34] The lattice constant of AlCoCrNiFe was 3.55 Å.[12] Initially, 10,000 FCC Fe atoms were created, and they were subsequently replaced with Ni, Cr, Co, and Al in a random manner based on a constant ratio. The crystal orientations are [100], [010], and [001]. Models with a length of 355 Å, and a width and height of 17.75×17.75 Å^2, were utilized. To achieve accurate simulation results in MD, the utilization of a suitable potential function is paramount. The Embedded Atom Method potential, as provided by Farks and Caro,[35] was chosen to accurately characterize the interactions among Al–Co–Cr–Fe–Ni atoms in the system. Subsequently, the steepest descent method was employed to minimize the energy of models of varying sizes. Finally, the whole system was relaxed under the canonical ensemble to obtain a more stable configuration.

B. Calculation of lattice thermal conductivity

In this study, the lattice thermal conductivity of HEAs at 300 K was calculated using the NEMD method. In the NEMD approach, aperiodic boundaries are implemented along the X direction and periodic boundaries along the Y and Z directions. The temperature of the hot and cold baths along the X direction was regulated using the Langevin thermostat, as shown in Fig. 1. The NEMD method causes the material to produce a stable temperature gradient by setting a heat and cold source in a specific direction. In accordance with Fourier's law, k_{P-MD} is determined by the following equation:

$$k_{p-MD} = -\frac{Jx}{dT/dx}, \tag{1}$$

where J_x is the heat flux generated by the hot and cold baths in the X direction and dT/dx is the temperature gradient generated.

C. Dataset establishment

A large, accurate, and evenly distributed data set is crucial for ML models because it can improve model accuracy and enhance its ability to generalize. The lattice thermal conductivity of 120 different compositions of HEAs was calculated using MD simulation. Due to the influence of the solid solubility of Al in HEAs, the Al content cannot be increased indefinitely. Currently, the Al content of HEAs reported in the literature is less than 10 at%.[36] In our dataset, the atomic percentage of Fe, Ni, Cr, and Co ranges from 20 at% to 25 at%, and the atomic percentage of Al ranges from 5 at% to 10 at%. Sun *et al.*[28] used MD simulation to establish an ideal disordered $Al_{0.3}CoCrNiFe$ model and calculated by the NEMD method that the lattice thermal conductivity of $Al_{0.3}CoCrNiFe$ is 3.5 W m^{-1} k^{-1} at 300 K. The lattice thermal conductivity of

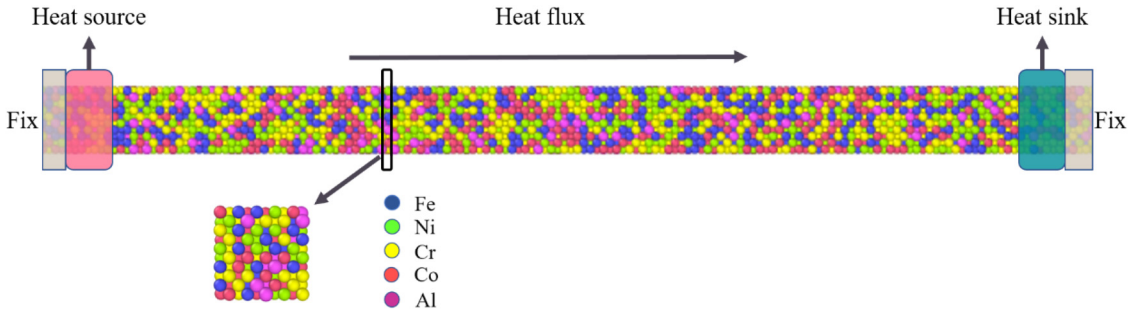

FIG. 1. The schematic of the NEMD method for calculating thermal conductivity.

Al0.3CoCrNiFe recorded in our dataset is 3.2 $W\,m^{-1}\,k^{-1}$, which is similar to the result reported in the literature. Our dataset records the atomic percentages of HEAs' composition, the model's size, and the lattice thermal conductivity calculated using MD. Due to the non-periodic boundary in the X direction of the model, the length in the X direction changes after the energy minimization and relaxation reach stability. Consequently, the length of the model is recorded in the dataset.

III. RESULTS AND DISCUSSION

A. Feature analysis

The five components of AlCoCrNiFe and the length of the model after relaxation were used as input values to predict the lattice thermal conductivity of HEAs when building an ML model in this study. The relationship between the input values and the lattice thermal conductivity of HEAs was analyzed by calculating the Pearson coefficients between six input values and the output value. Figure 2(a) demonstrates that the influence of Al on the lattice thermal conductivity of HEAs is more pronounced than that of other metal compositions. The negative correlation between the lattice thermal conductivity of Al and HEAs is evident from the negative Pearson coefficient. The lattice thermal conductivity of six groups of HEAs with varying compositions was calculated. Figure 2(b) reveals that the thermal conductivity of HEAs exhibits a decreasing trend with increasing Al content.

To gain a more profound understanding of our machine learning model's behavior, we conducted a sensitivity analysis using the Sobol sensitivity indices.[37] These indices quantify the influence of each input feature on the prediction of lattice thermal conductivity in HEAs. The calculated Sobol indices for the six input features—Al, Co, Cr, Ni, and Fe components, and the length of the model after relaxation—are presented in Fig. 3. The Sobol sensitivity indices reveal the relative importance of each input variable, providing a comprehensive understanding of their individual contributions to the lattice thermal conductivity predictions. Higher indices indicate a greater impact on the model's output. The calculated Sobol indices reveal varying degrees of impact, with input Cr exhibiting modest yet notable importance (Sobol's index = 0.523), closely followed by Fe (0.518), Co (0.514), and Ni (0.502). The remaining inputs, Al (0.621) and L (0.667), show slightly higher sensitivities, suggesting a relatively more pronounced role in shaping the predicted outcomes.

B. Model construction and evaluation

Choosing Support Vector Regression (SVR) in our study is grounded in its ability to handle non-linear relationships effectively.[38] Considering the intricate compositions and non-linear interactions present in HEAs, SVR proves advantageous in capturing the nuanced dependencies within our dataset. Its flexibility in discerning complex patterns aligns well with the challenges posed by HEA research, making it a suitable choice for predicting lattice thermal conductivity. In this study, we developed an SVR model capable of accurately predicting the lattice thermal conductivity of HEAs using the dataset of lattice thermal conductivity of HEAs simulated by MD. We perform data normalization in the dataset to

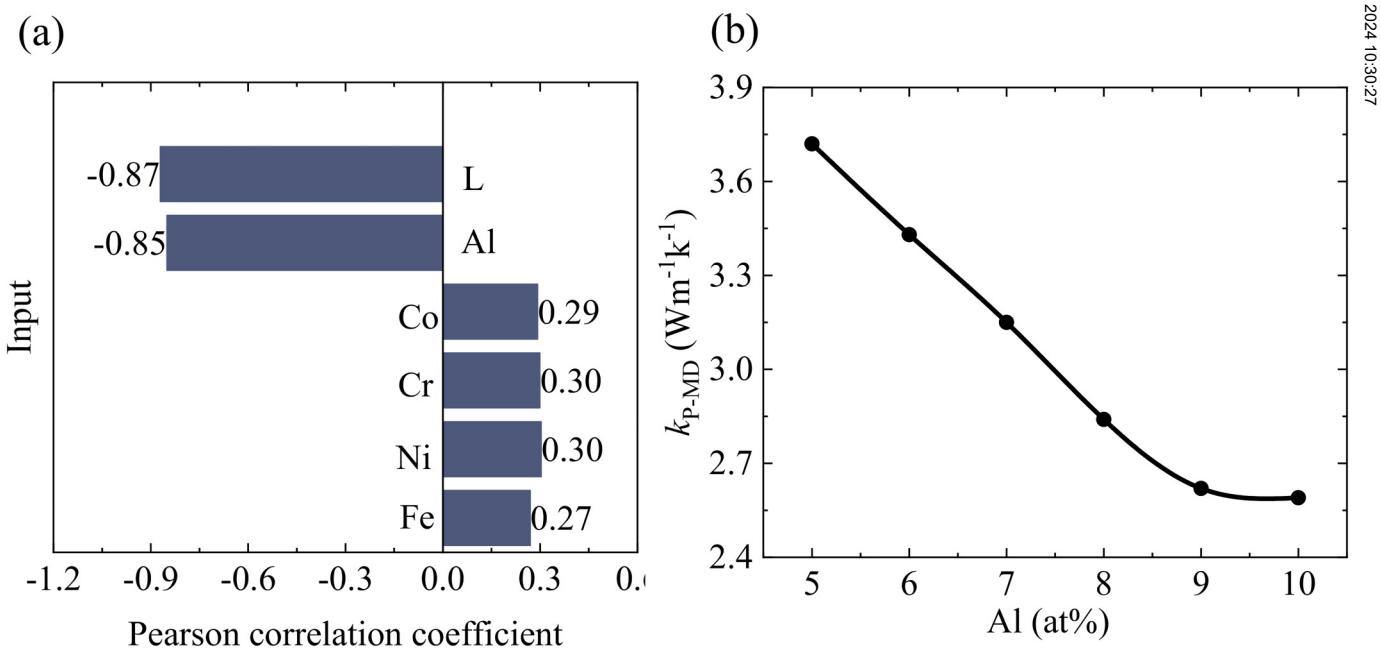

FIG. 2. (a) Pearson correlation coefficient between inputs and outputs. (b) The lattice thermal conductivity of AlCoCrNiFe (at. % Al = 5, 6, 7, 8, 9, 10). L denotes the length of the model after relaxed.

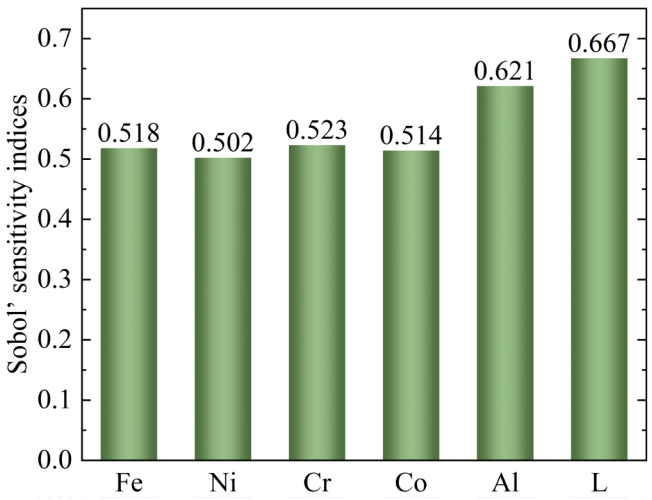

FIG. 3. Analysis of the Sobol sensitivity indices: Quantifying the impact of individual input variables on k_p prediction. L denotes the length of the model after relaxed.

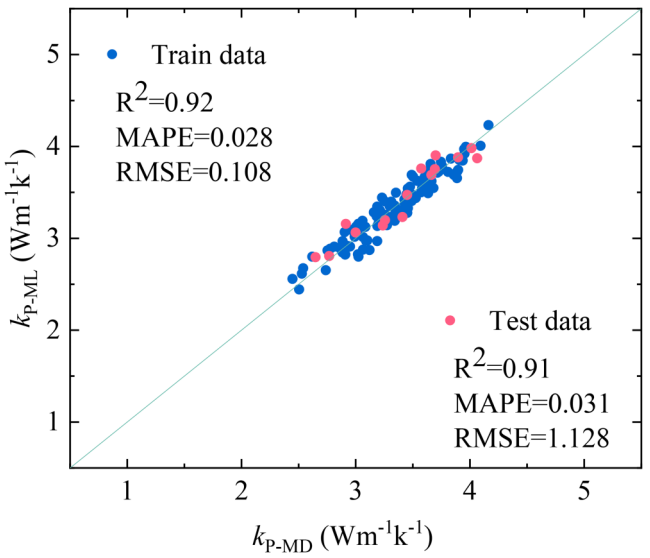

FIG. 4. Comparison between the k_{P-ML} predicted by the SVR model and the k_{P-MD} calculated by the MD. The units of RMSE are W m^{-1} k^{-1}.

transform the data into the range of (−1, 1), mitigating the impact of data range differences on the model training and enhancing the accuracy of the model's generalization ability. The dataset consists of 120 data, which are randomly divided into a training set with 115 data and a test set with 15 data. We optimized the parameters of the SVR model using a grid search optimization methodology in order to minimize the error between the predicted and calculated values on the test set. The trained SVR model is subsequently used to predict the test set data in order to evaluate the model's predictive ability and generalization capability.

The comparison results of the predicted and actual values for the training and test sets are depicted in Fig. 4. The data points for both the training set and testing set are distributed near the line y = x, without any outliers, indicating excellent predictive capability of the SVR model. By computing the coefficient of determination (R^2), mean absolute percentage error (MAPE), and root mean square error (RMSE) for both the training and testing sets, which can be calculated using Eqs. (2)–(4), we can effectively evaluate the predictive performance of the Support Vector Regression (SVR) model. These performance metrics play crucial roles in assessing the accuracy and reliability of machine learning models. Specifically, RMSE measures the absolute magnitude of deviation from the predicted value, while MAPE measures the relative magnitude of deviation. R^2 is commonly used to assess the goodness of fit of a regression model. Liu *et al.*[39] used a divide-and-conquer self-adaptive learning method for predicting creep rupture life in Ni-based single crystal superalloy materials. The R^2 value of 0.91 indicates high accuracy in predicting creep rupture life, showcasing the effectiveness of their approach. Wang *et al.*[40] focused on predicting thermal conductivity of crystal materials using machine learning models. The R^2 value reported in this study was 0.90, indicating a strong predictive capability for thermal conductivity based on crystal structural and compositional information. In contrast, our model outperforms existing models with an impressive R^2 of 0.92 for the training set and 0.91 for the test set. This represents a slight yet significant improvement, highlighting the efficacy of our approach. The small and close predictive errors of the SVR model for both the training set and testing set demonstrate the excellent generalization and fitting ability of the model,

$$RMSE = \sqrt{\sum_{i=1}^{n} \left(k^i_{p-ML} - k^i_{p-MD}\right)^2 / n}, \quad (2)$$

$$MAPE = \frac{1}{n} \frac{\sum_{i=1}^{n} \left|\left(k^i_{p-MD} - k^i_{p-ML}\right)\right|}{k^i_{p-MD}}, \quad (3)$$

$$R^2 = 1 - \frac{k^i_{p-MD} - k^i_{p-ML}}{k^i_{p-MD} - k^i_{p-avg}}, \quad (4)$$

where i specifies the material sample and n is the total number of samples in the dataset.

C. Prediction and validation of lattice thermal conductivity

The lattice thermal conductivity of HEAs has a complex relationship with its composition.[41] Although experimental measurement methods can obtain accurate lattice thermal conductivity, they involve complex processes and make it challenging to obtain the best HEAs. The NEMD simulation, based on interatomic interaction forces, can accurately predict the lattice thermal conductivity of HEAs.[42] However, the NEMD simulation requires considerable

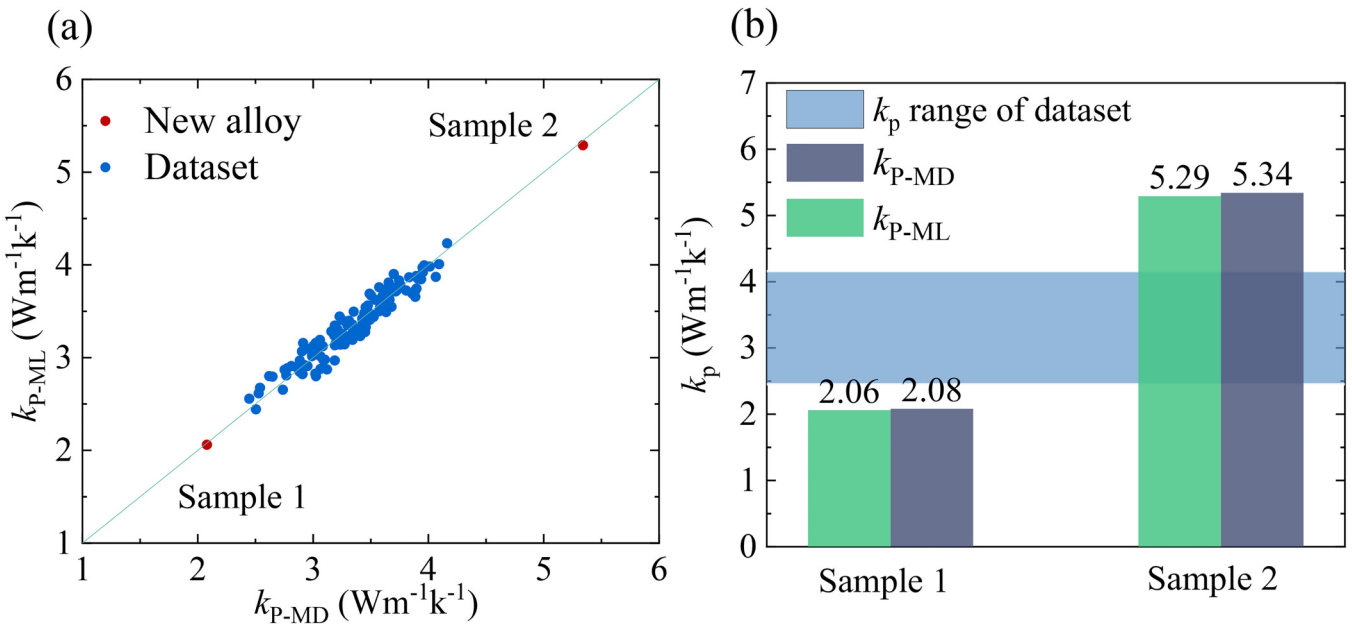

FIG. 5. (a) Comparison between the new alloys selected by the SVR model and other alloys of the dataset. (b) Comparison between the k_{P-ML} predicted by the SVR model and the k_{P-MD} calculated by NEMD for new alloys.

computational resources and time. In contrast, ML models can accurately predict the lattice thermal conductivity of HEAs in a short amount of time.[43] Therefore, sample 1 ($Al_8Cr_{30}Co_{19}Ni_{20}Fe_{23}$) with the lowest lattice thermal conductivity and sample 2 ($Al_{0.5}Cr_{28.5}Co_{25}Ni_{25.5}Fe_{20.5}$) with the highest lattice thermal conductivity were selected based on the SVR model within a reasonable range (0 at. % < Al < 20 at. %, 18 at. % < Cr < 27 at. %, 18 at. % < Co < 27 at. %, 18 at. % < Ni < 27 at. %, 18 at. % < Fe < 27 at. %),

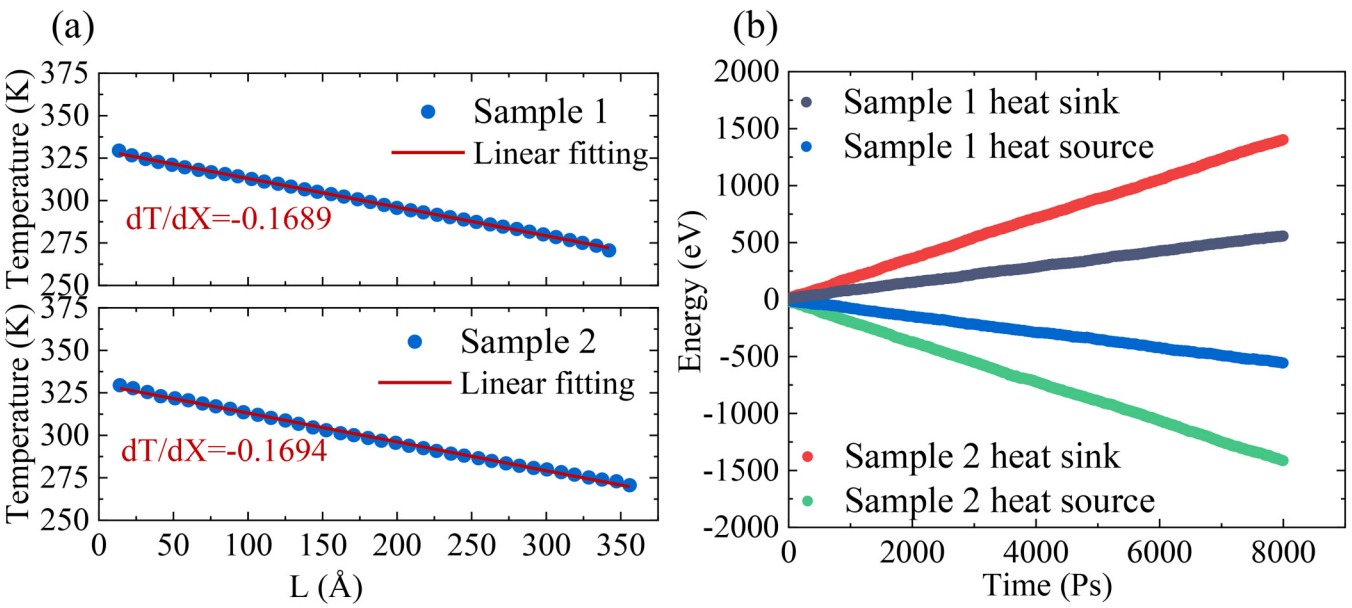

FIG. 6. (a) The temperature gradient in NEMD. (b) Exchanged energy of the heat source and heat sink over time.

TABLE I. Elemental content of sample 1 and sample 2.

	Fe (at. %)	Ni (at. %)	Cr (at. %)	Co (at. %)	Al (at. %)%	k_{P-MD} (W m^{-1} k^{-1})	k_{P-ML} (W m^{-1} k^{-1})
Sample 1	21.5	18	19.5	26	15	2.08	2.06
Sample 2	20.5	24.5	27	27	1	5.34	5.29

as shown in Fig. 5(a). Additionally, the lattice thermal conductivities of sample 1 and sample 2 were calculated using MD simulation to validate the accuracy of SVR model predictions. In the MD simulation, the Langevin controllers were used to control the temperatures at the left and right ends of the box at 270 and 330 K, respectively. Figure 6(a) shows the temperature gradient obtained from the lattice thermal conductivity calculations of HEA sample1 and sample2 using the NEMD method at 300 K. During the NEMD simulation, heat is continuously input at the left end and absorbed at the right end, resulting in the heat flux curve shown in Fig. 6(b). The linear fitting of the heat flux curve indicates that the heat flux density at both the hot and cold sources of sample 1 is 0.174 eV/ps, and the heat flux density at both the hot and cold sources of sample 2 is 0.069 eV/ps.

As shown in Fig. 5(b), HEA sample 1 with low lattice thermal conductivity is screened based on the SVR model. Its lattice thermal conductivity is 2.06 W m^{-1} k^{-1}, close to the NEMD simulation value of 2.08 W m^{-1} k^{-1}. Meanwhile, HEA sample 2 with high lattice thermal conductivity is screened based on the SVR model, and its lattice thermal conductivity is 5.29 W m^{-1} k^{-1}, close to the NEMD simulation value of 5.34 W m^{-1} k^{-1}. Table I lists the compositions of sample 1 and sample 2. The predicted values of the lattice thermal conductivity for HEA sample 1 and sample 2 by the SVR model are very close to the simulation values. This demonstrates that the trained compositional-property prediction model has good extrapolation capability to accurately predict the lattice thermal conductivity of HEAs outside the range of the dataset. Our model's ability to predict lattice thermal conductivity for untested compositions provides valuable insights for experimental design. Researchers can strategically use these predictions to guide their experimental efforts, focusing on alloy compositions that show the most promising thermal characteristics. This not only accelerates the experimental process but also contributes to resource efficiency in materials research.

D. Phonon transport mechanisms in AlCoCrNiFe

Analyzing the phonon density of states (PDOS) in HEAs provides crucial information about their thermal conductivity properties. By examining the shape and peak positions of the PDOS, specific phonon modes contributing to thermal conductivity can be determined.[22] Calculating the PDOS reveals the phonon transport mechanisms in HEAs, as shown in Fig. 7(a). The PDOS can be computed through the Fourier transform of the velocity

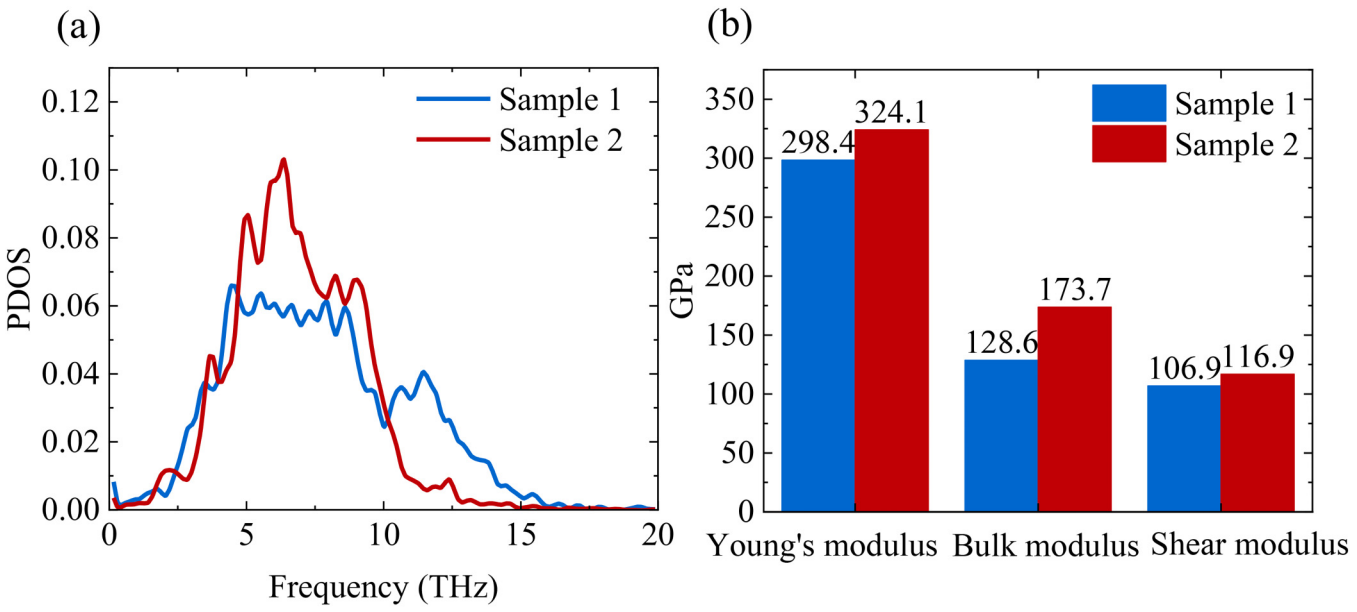

FIG. 7. (a) Comparison chat of PDOS of sample 1 (red line) and sample 2 (blue line). (b) Comparison chart of elastic modulus, bulk modulus, and shear modulus of sample 1 and sample 2.

autocorrelation function, which is expressed as

$$F(\omega) = \frac{1}{\sqrt{2\pi}} \int_{-\infty}^{+\infty} \frac{\langle v(0) \cdot v(t) \rangle}{\langle v(0) \cdot v(0) \rangle} e^{iwt} dt, \quad (5)$$

where v is the atomic velocity and the angle brackets represent the ensemble average. The higher $F(\omega)$ at a given frequency means that more phonons are involved in heat transport, leading to a higher thermal conductivity. As shown in Fig. 7(a), the PDOS of AlCoCrNiFe can be divided into two parts. The low-frequency range is within the 0–10 Hz range, and the high-frequency range is within the 10–20 Hz range. Sample 1 has lower Cr and Ni contents than sample 2, but the Al content is higher than sample 2. In AlCoCrNiFe, because the mass of the Al atom is lighter than that of the other four elements and its phonon energy level is lower, the contribution of the Al element to the PDOS is most significant in the low-frequency range.[23] Furthermore, in the low-frequency range, the PDOS of Al is lower than that of the other four elements. Therefore, in the low-frequency range, the PDOS of sample 2 is higher than that of sample 1. In the high-frequency range, the PDOS of the Cr element is the highest, while the PDOS of the Al element is the lowest.[44] Therefore, in the high-frequency range, the PDOS of sample 1 is higher. In AlCoCrNiFe, the mass of Al atoms is lighter than other elements. With increased Al content, the uneven distribution of atomic mass becomes more significant, enhancing phonon scattering and reducing the lattice thermal conductivity. The Al content in sample 1 is 15 at. %, much higher than that of sample 2; thus, the mass mismatch in sample 2 leads to increased phonon scattering and decreasing lattice thermal conductivity. It is consistent with the calculated result that the lattice thermal conductivity of sample 1 is lower than that of sample 2.

The elastic modulus, shear modulus, and bulk modulus of HEAs are well associated with lattice thermal conductivity.[45] Diversity and randomness of elements in AlCoCrNiFe lead to a more complex lattice structure, which affects phonon transport and vibrational modes. As shown in Fig. 7(b), MD simulation was used to calculate the elastic modulus, bulk modulus, and shear modulus of the HEA sample 1 and sample 2. The results show that the high-entropy alloy sample 2 has a high elastic modulus, bulk modulus, and shear modulus. A higher elastic modulus means that the lattice vibrations of sample 2 are more coordinated and the atomic structure is more tightly ordered. This promotes phonon conduction and enhances lattice thermal conductivity.

IV. CONCLUSIONS

In summary, ML and MD simulations were combined to predict the lattice thermal conductivity of AlCoCrNiFe. Our SVR model shows high accuracy with the R^2 of the test set is 0.91 and the R^2 of the train set is 0.92. By calculating the Pearson coefficients between composition and lattice thermal conductivity, it is found that the change in the Al content has the most significant impact on the lattice thermal conductivity compared to Fe, Ni, Cr, and Co. However, HEAs with a low lattice thermal conductivity of 2.06 $W\,m^{-1}\,k^{-1}$ ($Al_8Cr_{30}Co_{19}Ni_{20}Fe_{23}$) and with a high lattice thermal conductivity of 5.29 $W\,m^{-1}\,k^{-1}$ ($Al_{0.5}Cr_{28.5}Co_{25}Ni_{25.5}Fe_{20.5}$) were successfully predicted, which show a good agreement with the results from MD simulations. Calculating the density of phonon states of sample 1 and sample 2 shows that the PDOS of AlCoCrNiFe can be divided into two parts. In the low-frequency range, the PDOS of sample 2 is higher than that of sample 1, but in the high-frequency range, the PDOS of sample 1 is higher. The higher elastic modulus of sample 2 means that the lattice vibrations are more coordinated and the atomic structure is more tightly ordered. This promotes phonon conduction and enhances lattice thermal conductivity.

ACKNOWLEDGMENTS

This study was financially supported by the National Key Research and Development Program of China (No. SQ2023YFE0102578) and the National Natural Science Foundation of China (NNSFC) (No. 52076156). The authors appreciate the support from the Supercomputing Center of Wuhan University.

AUTHOR DECLARATIONS

Conflict of Interest

The authors have no conflicts to disclose.

Author Contributions

Jie Lu: Data curation (equal); Investigation (equal); Methodology (equal); Software (equal); Writing – original draft (equal). **Xiaona Huang:** Resources (equal); Software (equal); Supervision (equal); Writing – review & editing (equal). **Yanan Yue:** Supervision (equal); Validation (equal).

DATA AVAILABILITY

The data that support the findings of this study are available from the corresponding authors upon reasonable request.

REFERENCES

[1]S. Chen, T. Wang, X. Li, Y. Cheng, G. Zhang, and H. Gao, "Short-range ordering and its impact on thermodynamic property of high-entropy alloys," Acta Mater. **238**, 118201 (2022).
[2]S. Yang, J. Lu, F. Xing, L. Zhang, and Y. Zhong, "Revisit the VEC rule in high entropy alloys (HEAs) with high-throughput CALPHAD approach and its applications for material design—A case study with Al–Co–Cr–Fe–Ni system," Acta Mater. **192**, 11 (2020).
[3]Y. Wang, X. Huang, Y. Liu, X. Zhang, B. Yang, and Y. Yue, " Thermal and mechanical characterization of under-2-μm-thick AlCrNbSiTi high-entropy thin film," Energy Storage Sav. **3**, 52 (2024).
[4]C. Wang, X. Zhou, D. Cong, G. Tang, and J. Yang, "A novel valence-balanced double half-Heusler $Ti_2Zr_2Hf_2NbVFe_5Ni_3Sb_8$ alloy by high entropy engineering," Mater. Today Phys. **36**, 101172 (2023).
[5]W. Li, D. Xie, D. Li, Y. Zhang, Y. Gao, and P. K. Liaw, "Mechanical behavior of high-entropy alloys," Prog. Mater. Sci. **118**, 100777 (2021).
[6]Q. Sun, Z. Xue, Y. Chen, R. Xia, J. Wang, S. Xu, J. Zhang, and Y. Yue, "Modulation of the thermal transport of micro-structured materials from 3D printing," Int. J. Extreme Manuf. **4**, 015001 (2021).
[7]C. Wagner, A. Ferrari, J. Schreuer, J. P. Couzinié, Y. Ikeda, F. Körmann, G. Eggeler, E. P. George, and G. Laplanche, "Effects of Cr/Ni ratio on physical properties of Cr-Mn-Fe-Co-Ni high-entropy alloys," Acta Mater. **227**, 117693 (2022).

[8]X. Yan, L. Constantin, Y. Lu, J. F. Silvain, M. Nastasi, and B. Cui, "$(Hf_{0.2}Zr_{0.2}Ta_{0.2}Nb_{0.2}Ti_{0.2})C$ high-entropy ceramics with low thermal conductivity," J. Am. Ceram. Soc. **101**, 4486–4491 (2018).
[9]C. M. Rost, T. Borman, M. D. Hossain, M. Lim, K. F. Quiambao-Tomko, J. A. Tomko, D. W. Brenner, J. P. Maria, and P. E. Hopkins, "Electron and phonon thermal conductivity in high entropy carbides with variable carbon content," Acta Mater. **196**, 231–239 (2020).
[10]X. Huang, J. Guo, and Y. Yue, "Graphene coated 3C-SiC with improved irradiation resistance and enhanced heat conduction property after collision cascade," Int. J. Heat Mass Transfer **194**, 122988 (2022).
[11]L. Hu, Y. Zhang, H. Wu, J. Li, Y. Li, M. McKenna, J. He, F. Liu, S. J. Pennycook, and X. Zeng, "Entropy engineering of SnTe: Multi-principal-element alloying leading to ultralow lattice thermal conductivity and state-of-the-Art thermoelectric performance," Adv. Energy Mater. **8**, 1802116 (2018).
[12]G. Kim, H. Diao, C. Lee, A. T. Samaei, T. Phan, M. de Jong, K. An, D. Ma, P. K. Liaw, and W. Chen, "First-principles and machine learning predictions of elasticity in severely lattice-distorted high-entropy alloys with experimental validation," Acta Mater. **181**, 124–138 (2019).
[13]P. C. Wei, C. N. Liao, H. J. Wu, D. Yang, J. He, G. V. Biesold, S. Liang, W. T. Yen, X. Tang, J. W. Yeh, Z. Lin, and J. H. He, "Thermodynamic routes to ultralow thermal conductivity and high thermoelectric performance," Adv. Mater. **32**, 1906457 (2020).
[14]G. Qin, Y. Wei, L. Yu, J. Xu, J. Ojih, A. D. Rodriguez, H. Wang, Z. Qin, and M. Hu, "Predicting lattice thermal conductivity from fundamental material properties using machine learning techniques," J. Mater. Chem. A **11**, 5801–5810 (2023).
[15]X. Huang, C. Li, K. Tan, Y. Wen, F. Guo, M. Li, Y. Huang, C. Q. Sun, M. Gozin, and L. Zhang, "Applying machine learning to balance performance and stability of high energy density materials," iScience **24**, 102240 (2021).
[16]S. Wu, Y. Kondo, M. A. Kakimoto, B. Yang, H. Yamada, I. Kuwajima, G. Lambard, K. Hongo, Y. Xu, J. Shiomi, C. Schick, J. Morikawa, and R. Yoshida, "Machine-learning-assisted discovery of polymers with high thermal conductivity using a molecular design algorithm," npj Comput. Mater. **5**, 66 (2019).
[17]C. Shen, C. Wang, X. Wei, Y. Li, S. van der Zwaag, and W. Xu, "Physical metallurgy-guided machine learning and artificial intelligent design of ultrahigh-strength stainless steel," Acta Mater. **179**, 201–214 (2019).
[18]C. T. Wu, H. T. Chang, C. Y. Wu, S. W. Chen, S. Y. Huang, M. Huang, Y. T. Pan, P. Bradbury, J. Chou, and H. W. Yen, "Machine learning recommends affordable new Ti alloy with bone-like modulus," Mater. Today **34**, 41–50 (2020).
[19]W. Huang, P. Martin, and H. L. Zhuang, "Machine-learning phase prediction of high-entropy alloys," Acta Mater. **169**, 225–236 (2019).
[20]H. Zhang, H. Fu, X. He, C. Wang, L. Jiang, L. Q. Chen, and J. Xie, "Dramatically enhanced combination of ultimate tensile strength and electric conductivity of alloys via machine learning screening," Acta Mater. **200**, 803–810 (2020).
[21]J. Li, Y. Zhang, X. Cao, Q. Zeng, Y. Zhuang, X. Qian, and H. Chen, "Accelerated discovery of high-strength aluminum alloys by machine learning," Commun. Mater. **1**, 73 (2020).
[22]W. Liu, X. Huang, and Y. Yue, "Tuning thermal transport across monolayer MoS_2/Si heterostructure via substrate nanogrooving," Int. J. Heat Mass Transfer **201**, 123673 (2023).
[23]M. A. A. Hasan, J. Wang, S. Shin, D. A. Gilbert, P. K. Liaw, N. Tang, W. L. N. C. Liyanage, L. Santodonato, L. D. Schmitt, and N. P. Butch, "Effects of aluminum content on thermoelectric performance of Al CoCrFeNi high-entropy alloys," J. Alloys Compd. **883**, 160811 (2021).
[24]C. Wang, H. Fu, L. Jiang, D. Xue, and J. Xie, "A property-oriented design strategy for high performance copper alloys via machine learning," npj Comput. Mater. **5**, 87 (2019).
[25]M. Caro, L. K. Béland, G. D. Samolyuk, R. E. Stoller, and A. Caro, "Lattice thermal conductivity of multi-component alloys," J. Alloys Compd. **648**, 408–413 (2015).
[26]N. Birbilis, M. K. Cavanaugh, A. D. Sudholz, S. M. Zhu, M. A. Easton, and M. A. Gibson, "A combined neural network and mechanistic approach for the prediction of corrosion rate and yield strength of magnesium-rare earth alloys," Corros. Sci. **53**, 168–176 (2011).
[27]C. Loftis, K. Yuan, Y. Zhao, M. Hu, and J. Hu, "Lattice thermal conductivity prediction using symbolic regression and machine learning," J. Phys. Chem. A **125**, 435–450 (2020).
[28]Z. Sun, C. Shi, L. Gao, S. Lin, and W. Li, "Thermal physical properties of high entropy alloy $Al_{0.3}$CoCrFeNi at elevated temperatures," J. Alloys Compd. **901**, 163554 (2022).
[29]S. Riniker, "Molecular dynamics fingerprints (MDFP): Machine learning from MD data To predict free-energy differences," J. Chem. Inf. Model. **57**, 726–741 (2017).
[30]X. Huang, Y. J. Hu, and Q. An, "Locking of screw dislocations in silicon due to core structure transformation," J. Phys. Chem. C **125**, 24710–24718 (2021).
[31]X. Gu, Z. Fan, and H. Bao, "Thermal conductivity prediction by atomistic simulation methods: Recent advances and detailed comparison," J. Appl. Phys. **130**, 210902 (2021).
[32]P. Roy Chowdhury and X. Ruan, "Unexpected thermal conductivity enhancement in aperiodic superlattices discovered using active machine learning," npj Comput. Mater. **8**, 99–105 (2022).
[33]J. Yan, P. Gorai, B. Ortiz, S. Miller, S. A. Barnett, T. Mason, V. Stevanović, and E. S. Toberer, "Material descriptors for predicting thermoelectric performance," Energy Environ. Sci. **8**, 983–994 (2015).
[34]M. Bahramyan, R. T. Mousavian, and D. Brabazon, "Determination of atomic-scale structure and compressive behavior of solidified Al_xCrCoFeCuNi high entropy alloys," Int. J. Mech. Sci. **171**, 105389 (2020).
[35]D. Farkas and A. Caro, "Model interatomic potentials for Fe–Ni–Cr–Co–Al high-entropy alloys," J. Mater. Res. **35**, 3031–3040 (2020).
[36]Z. U. Arif, M. Y. Khalid, E. ur Rehman, S. Ullah, M. Atif, and A. Tariq, "A review on laser cladding of high-entropy alloys, their recent trends and potential applications," J. Manuf. Proc. **68**, 225–273 (2021).
[37]P. Wei, Z. Lu, and J. Song, "Regional and parametric sensitivity analysis of Sobol indices," Reliab. Eng. Syst. Safety **137**, 87–100 (2015).
[38]M. Hu, Q. Tan, R. Knibbe, M. Xu, B. Jiang, S. Wang, X. Li, and M.-X. Zhang, "Recent applications of machine learning in alloy design: A review," Mater. Sci. Eng.: R: Rep. **155**, 100746 (2023).
[39]Y. Liu, J. Wu, Z. Wang, X. G. Lu, M. Avdeev, S. Shi, C. Wang, and T. Yu, "Predicting creep rupture life of Ni-based single crystal superalloys using divide-and-conquer approach based machine learning," Acta Mater. **195**, 454–467 (2020).
[40]X. Wang, S. Zeng, Z. Wang, and J. Ni, "Identification of crystalline materials with ultra-low thermal conductivity based on machine learning study," J. Phys. Chem. C **124**, 8488–8495 (2020).
[41]O. K. Orhan, M. Isiet, L. Caparini, and M. Ponga, "Exploring the compositional space of high-entropy alloys for cost-effective high-temperature applications," Front. Mater. **8**, 816610 (2022).
[42]S. Arabha, Z. S. Aghbolagh, K. Ghorbani, S. M. Hatam-Lee, and A. Rajabpour, "Recent advances in lattice thermal conductivity calculation using machine-learning interatomic potentials," J. Appl. Phys. **130**, 210903 (2021).
[43]Y. Du, P. Ying, and J. Zhang, "Prediction and optimization of the thermal transport in hybrid carbon-boron nitride honeycombs using machine learning," Carbon **184**, 492–503 (2021).
[44]H. Song, Q. Ma, W. Zhang, and F. Tian, "Effects of vacancy on the thermodynamic properties of Co-Cr-Fe-Mn-Ni high-entropy alloys," J. Alloys Compd. **885**, 160944 (2021).
[45]G. Laplanche, M. Schneider, F. Scholz, J. Frenzel, G. Eggeler, and J. Schreuer, "Processing of a single-crystalline CrCoNi medium-entropy alloy and evolution of its thermal expansion and elastic stiffness coefficients with temperature," Scr. Mater. **177**, 44–48 (2020).